ACS OMEGA

Open Access

http://pubs.acs.org/journal/acsodf

Article

Synthesis of Bovine Serum Albumin-Coated Magnetic Single-Walled Carbon Nanotubes as a Delivery System for Mitoxantrone

Buğçe Aydın, Serdar Bozoğlu, Nilgün Karatepe, and F. Seniha Güner*

Cite This: *ACS Omega* 2025, 10, 102−113

Read Online

ACCESS | Metrics & More | Article Recommendations | Supporting Information

ABSTRACT: In this study, a bovine serum albumin (BSA)-coated magnetic single-walled carbon nanotube (mCNT) was synthesized using covalent functionalization. Mitoxantrone (MTO) was chosen as a model drug, and loading/release profiles of mCNTs were evaluated. To synthesize BSA-coated mCNT, 1-ethyl-3-(3-(dimethylamino)propyl) carbodiimide and *N*-hydroxysuccinimide were used as cross-linking agents. The success of the functionalization process was demonstrated through various analysis techniques such as Fourier transform infrared spectroscopy, Raman spectroscopy, thermogravimetric analysis, X-ray photoelectron spectroscopy, vibrating sample magnetometer, and scanning electron microscopy. The saturation magnetization of mCNT-BSA was 15.6 emu/g, indicating its potential for magnetically targeted drug delivery systems. Finally, MTO was physically loaded on the BSA-coated mCNT (mCNT-BSA) and the results were compared to those of mCNT. mCNT-BSA showed less drug loading capacity but more release response than mCNT. Considering drug release and cytotoxicity test results, MTO-loaded mCNT-BSA nanoparticles have great potential for cancer treatment.

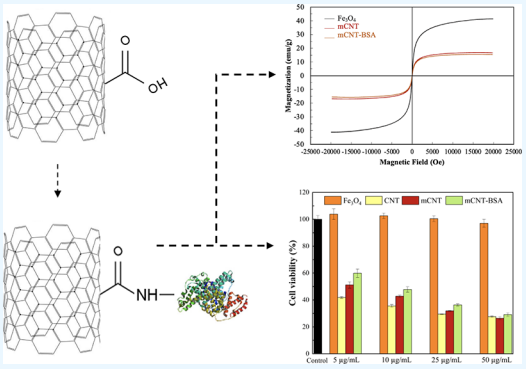

INTRODUCTION

Cancer is the second main cause of deaths worldwide.[1,2] Traditional cancer treatment approaches are chemotherapy, radiotherapy, and surgery. Although chemotherapy is one of the most effective treatments, anticancer drugs are toxic to both tumor cells and normal cells, so the efficiency of chemotherapy is often limited by significant side effects such as bone marrow suppression, hair loss, anemia, and poor solubility of drugs.[3] Recently, advanced drug delivery systems have been developed as cancer treatment methods.[2,4]

Magnetic nanoparticles (MNPs) are the most promising delivery system, which can be targeted to the tumor site using a magnetic field to decrease the undesirable side effect.[5] In addition, MNPs generate heat and raise the temperature of the cancerous region up to 42−46 °C. At these temperatures, tumor cells die, as they have lower heat resistance than normal cells.[6−8] Previous studies have demonstrated that magnetic nanocarriers may be more effective for cancer treatment under a magnetic field compared to nonmagnetic nanomaterials. Those studies indicated that magnetic nanocarrier systems exhibited higher efficiency in enhancing cytotoxicity than free drug and enhanced tumor-targeting ability and release in the tumor site.[9−12] Delivery of anticancer drugs by MNPs can overcome the disadvantages associated with common chemotherapeutic agents. CNTs are very encouraging delivery carriers for anticancer drug delivery systems, and they can combine with MNPs. mCNT can be targeted and concentrated in a specific zone using magnetic force, resulting in higher local drug concentration. Both passive and magnetic field effect targeting will ensure the destruction of tumor cells in the targeted area with a smaller amount of drugs, while the toxic effect on normal cells can also be reduced.[13,14] CNTs are carbon cylinders composed of benzene rings. The properties of CNT such as high mechanical strength, high surface area, the ability to pass through the cell membrane, pH-dependent drug release, high drug loading capacity, and easy modification lead to being a suitable carrier in drug delivery systems.[15,16] Nonfunctional CNTs were originally hydrophobic and toxic. To overcome these drawbacks, modification of a CNT surface has been mediated by two different strategies, noncovalent and covalent functionalization, that render them hydrophilic. Recently, carbon nanotubes were modified using polyethylenimine, chitosan, polyethylene glycol (PEG), and bovine serum albumin (BSA) by noncovalent[17−19] and covalent[20−25] functionalizing methods. A noncovalent bond is sensitive to environmental factors and more unstable compared to a covalent bond.[24] In addition, covalent functionalization is a more sensible and proper approach for biomedical applications.[21,26] In covalent

Received: December 1, 2023
Revised: July 9, 2024
Accepted: July 31, 2024
Published: January 1, 2025

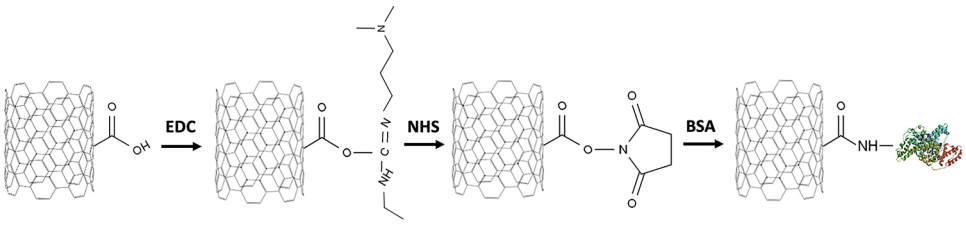

Figure 1. Schematic representation of the preparation of mCNT-BSA.

approaches, a chemical bond can be achieved between the surface of CNTs and biomolecules via the functionalization of sidewalls or ends of CNT.[27]

Proteins are an essential group of organic structures used to improve the biocompatibility of nanocarriers. Among the proteins, albumin is the most abundant protein in the plasma[28,29] and has attracted attention in virtue of its solubility in water, biodegradability, and nontoxicity.[30,31] The structural configuration of BSA provides various ligand binding sites and BSA can significantly decrease the cytotoxicity of CNTs.[32] In covalent conjugation, BSA can be easily attached to the surface of CNT by using cross-linking agents, which form an amide bond between the CNT and BSA. Many researchers have studied albumin-based nanoparticles for drug delivery systems in the literature. In a study performed by Salehiabar et al.,[30] BSA nanoparticles were synthesized for curcumin delivery. The nanocarrier had much higher cytotoxicity against cancer cells due to sustained drug release. In another study,[33] lapatinib-loaded albumin-coated polylactic-*co*-glycolic acid nanoparticles exhibited improved colloidal stability, greater cellular uptake, and a pH-responsive controlled drug release profile.

MTO is an anthracenedione-based anticancer drug and is commonly used for cancer therapy. Unfortunately, MTO is associated with side effects such as severe cardiotoxicity, a decrease in white blood cells, and amenorrhea due to the nonspecific effects of MTO.[34] However, this drug has fewer acute side effects including alopecia, nausea, and vomiting compared to other chemotherapeutic agents.[35−38] For the past decade, different nanoparticles have been designed as drug delivery carriers for anticancer drug MTO.[34,38−40] Wani et al.[41] reported the application of PEGylated mesoporous silica nanorods for the delivery of MTO. The drug loading and release studies highlighted that PEGylation of mesoporous silica nanorods decreased the MTO loading but increased MTO release compared to non-PEGylated nanocarriers. Sargazi et al.[42] used HA-PEGylated MNPs as a drug delivery carrier. It was found that only 33 and 6.1% of MTO were released at pH 5.0 and 7.4, respectively. In another study,[43] carboxylated graphene quantum dots were synthesized with PEG and folic acid by covalent modification and used for a new drug delivery system. Almost 38.3% of the total drug was released at pH 5.3, which was increased by approximately 130% compared with 16.5% at pH 7.3.

In recent years, studies in which various cancer drugs such as gemcitabine,[44] doxorubicin,[45] tamoxifen,[46] and methotrexate[47] were loaded on synthesized BSA nanoparticles have been reported in the literature. To our knowledge, there has been no previous study on the delivery of an MTO drug with a magnetic single-walled carbon nanotube nanocarrier, in which BSA is functionalized by covalent bonding. Based on this motivation, in this study, MTO-loaded magnetic single-walled CNT was modified to utilize an external stimuli system to reach tumor tissue. Carboxylated mCNTs were functionalized with BSA by covalent modification. BSA-coated mCNT was characterized by advanced analysis techniques, and its suitability was determined for the intended use. MTO as a model drug was loaded onto the nanocarriers, and a two-stage study was conducted for cytotoxicity tests. First, the cytotoxicity effects of nanocarriers were examined in a healthy cell line (HEK293T), and then MTO-loaded nanocarriers were studied in a cancer cell line (MDA-MB-231). A magnetic drug delivery carrier based on mCNT-BSA nanoparticles was developed with demonstrated advantages such as high drug release and magnetic targeting. Their superparamagnetic property enables the drug carrier to deliver drugs to the targeted site by applying external magnetic fields, which can achieve the restrictions of conventional cancer therapy.

MATERIALS AND METHODS

Materials. Iron(III) chloride ($FeCl_3$), iron(II) sulfate heptahydrate ($FeSO_4{\cdot}7H_2O$), ammonium hydroxide (NH_4OH), protocatechuic acid (PCA), BSA, 1-ethyl-3-(3-(dimethylamino)propyl) carbodiimide (EDC), and *N*-hydroxysuccinimide (NHS) were obtained from Sigma-Aldrich. Tetrahydrofuran (THF; anhydrous, ≥99.9%), nitric acid (HNO_3; 65%), and mitoxantrone dihydrochloride were also purchased from Sigma-Aldrich.

Synthesis and Coating of Iron Oxide Nanoparticles. Iron oxide nanoparticles (IONPs) were synthesized through coprecipitation of iron salts similar to a previously reported study.[48] $FeCl_3$ and $FeSO_4{\cdot}7H_2O$ were dissolved in 54 mL of deionized water. At 25 °C, NH_4OH was added to the solution. The solution was magnetically stirred for 2 min to precipitate the IONPs. The precipitate was separated with the help of a magnet, decanted, and washed with pure water until the pH reached a neutral level. Finally, the sample was dried by using a freeze-dryer for 24 h.

IONPs were coated with PCA, also known as 3,4-dihydroxybenzoic acid, to endow nanoparticles with colloidal stability in organic solvents. The nanoparticles obtained in the coprecipitation method were added to the ammonium hydroxide solution prepared. After mixing for a while with the help of a mechanical stirrer, PCA was added to the solution, and the mixing continued for another 15 min at 1000 rpm. Coated MNPs were separated with a magnet. The sample was washed with distilled water and ethanol to remove ammonium hydroxide and excess PCA. It was freeze-dried for 24 h.

Synthesis and Modification of Single-Walled Carbon Nanotubes with IONPs. Single-walled carbon nanotubes (SWNTs) were synthesized by a chemical vapor deposition method according to our previously reported procedure.[49] Briefly, a magnesium oxide (100 $m^2{\cdot}g^{-1}$)-supported iron oxide powder produced by impregnation in an iron nitrate/ethanol solution was used as a precursor powder. Then, the furnace was heated to 800 °C. The synthesis was started with the introduction of acetylene mixed with argon and lasted for 30

https://doi.org/10.1021/acsomega.3c09608
ACS Omega 2025, 10, 102−113

min. After synthesis, SWNTs were purified with 6 M HNO_3 for 3 h.

Magnetically modified SWNTs were prepared by the ligand exchange method. SWNTs were dispersed for 30 min in 20 mL of THF with the help of an ultrasonic probe. A second solution was prepared in 15 mL of THF with PCA-coated IONPs. This solution was added to the SWNT solution with a ratio of 2 to 1 wt (SWNTs/IONPs) and stirred at 700 rpm for 6 h. Modified CNTs (mCNTs) were collected with a magnet and freeze-dried for 24 h.

Covalent Functionalization of mCNTs with BSA. mCNT was added to a phosphate buffer solution (PBS) and kept for 30 min under constant stirring. EDC (125 mg) and NHS (75 mg) were added to the above solution to activate the carboxyl groups in mCNT. The mixture was stirred using a mechanical stirrer for 2 h. Then, 75 mg of BSA was added, and the mixing condition was continued for 24 h in a dark room. As depicted in Figure 1, BSA was linked to mCNT via reaction between the $-NH_2$ of BSA and the $-COOH$ of mCNT. The nanocarrier was separated using a magnet, washed with distilled water, and then dried in a vacuum oven at 40 °C. BSA-functionalized mCNTs will be termed mCNT-BSA henceforth.

Characterization. The Fourier transform infrared (FT-IR) spectrum was obtained using an FT-IR/ATR, PerkinElmer-Spectrum Two instrument in the wavenumber range of 800−4000 cm^{-1}. Raman measurements were performed using a Renishaw inVia Raman microscope with excitation at 532 nm. X-ray diffraction (XRD) analysis was performed on SmartLab, Rigaku using 1.5406 nm Cu Kα radiation. The diffraction angle (2θ) was recorded from 10 to 90° with a scanning speed of 1.5°/min. Thermogravimetric analysis (TGA) was carried out using a thermogravimetric analyzer (Q600 SDT, TA Instruments) in air and nitrogen atmosphere at a heating rate of 10 °C/min. A vibrating sample magnetometer (VSM, Lake Shore 7407) was used to measure the magnetic properties of the nanocarriers at room temperature. The chemical composition of the samples was analyzed by PHI VersaProbe 5000 scanning X-ray photoelectron spectroscopy (XPS). The morphology of samples was obtained by field emission scanning electron microscopy (FEG-SEM, FEI Quanta FEG 450) and scanning electron microscopy (SEM, JEOL-JSM7001F) equipped with energy-dispersive X-ray spectroscopy (EDS).

The carboxylated CNTs were analyzed by a titration method to evaluate the $-COOH$ contents on the surface of CNTs. In the experiment, the samples were dispersed in 25 mL of 0.04 N NaOH solution and stirred for 48 h. Then, the mixture was titrated with 0.04 N HCl.[50] Each sample was made in triplicate.

MTO Loading and Release. The nanocarrier (3 mg) was added to the drug solutions (0.1 mg/mL) in PBS (pH 9). The mixture was stirred in an orbital shaker at 25 °C for 48 h in the dark. After the mCNTs were separated with a magnet, nanocarriers were washed with PBS twice to remove the remaining MTO around the mCNTs. To find the amount of unloaded MTO, measurements were taken at 611 nm using a UV−vis spectrophotometer (Cary 60, Agilent Technologies). Concentration values were calculated with the calibration curve at pH 9 (Figure S1) to determine the amount of MTO in the solution. Drug loading efficiency and drug loading content were calculated by using eqs 1 and 2, respectively.

$$\text{drug loading efficiency (\%)} = \frac{\text{mass of loaded MTO (mg)}}{\text{total MTO (mg)}} \times 100 \quad (1)$$

$$\text{drug loading content} = \frac{\text{mass of loaded MTO (μg)}}{\text{mass of nanocarrier (mg)}} \quad (2)$$

Drug release studies were performed in PBS at pH 5.5 and 7.4. For this purpose, 3 mg of MTO-loaded mCNTs was dissolved in 10 mL of PBS at 37 °C. At desired time intervals, samples were separated from the solution media, and the amount of drug in the solution was monitored by a UV−vis spectrophotometer at 611 nm. The absorbance measurements were converted to the concentration values using the different calibration curves for pH 5.5 (Figure S2) and 7.4 (Figure S3). Cumulative drug release percentage was calculated using eq 3.

$$\text{cumulative release of MTO (\%)} = \frac{\text{mass of the released MTO (mg)}}{\text{mass of MTO in nanocarrier (mg)}} \times 100 \quad (3)$$

In Vitro Cytotoxicity Assay. The cytotoxic effects of functionalized nanocarriers were examined on human embryonic kidney (HEK293T) and human breast cancer (MDA-MB-231) cell lines using the MTT assay. For the MTT test, cells were seeded in 96-well plates at a density of 2500 cells/well. Then, the cells were treated with different concentrations of nanocarriers for 48 h. Following the incubation, the MTT agent (5 mg/mL) was added to the wells. After 4 h of incubation, the color change resulting from formazan formation was measured spectrophotometrically (BioTek 800 TS) at 570 nm. Cell viabilities (%) were calculated using the values for the control group. In addition, cell studies of MTO-loaded mCNTs on MDA-MB-231 were repeated by placing a magnet at the bottom of 96-well plates. All experiments were performed in triplicate. Absorbance data were analyzed using GraphPad Prism 7.0 compared to the control cells.

Statistical Analysis. Statistical analysis was performed with the one-way analysis of variance (ANOVA), Student's t test, and Tukey's multiple comparisons test. Differences were considered significant from $p \leq 0.05$. All results are expressed as the mean ± standard deviation.

RESULTS AND DISCUSSION

mCNT Characterization. Raman spectroscopy was performed for the carboxylated CNT and mCNT; analysis results are listed in Table 1. The intensity ratio of the D and G bands (I_D/I_G) indicates the quality of synthesized CNTs. The intensity of the G band is higher than that of the D band for nanocarriers. I_D/I_G ratios for carboxylated CNT and mCNT were found to be 0.28 and 0.47, respectively. The significant increase in this ratio suggests the increase in the defects in the structure and the decrease in the amount of the sp^2 domains.[51,52] The RBM band

Table 1. Peak Positions of RBM and D and G Bands for Carboxylated CNT and mCNT

	Raman shift (cm^{-1})			
sample	RBM	D	G	I_D/I_G
carboxylated CNT	165, 266	1339	1580	0.28
mCNT	128, 176	1343	1580	0.47

https://doi.org/10.1021/acsomega.3c09608
ACS Omega 2025, 10, 102−113

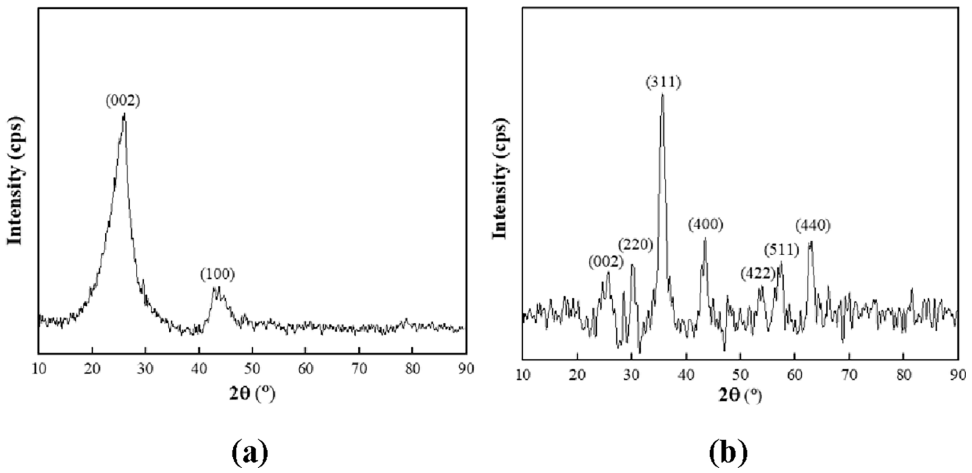

Figure 2. XRD spectra of (a) carboxylated CNT and (b) mCNT.

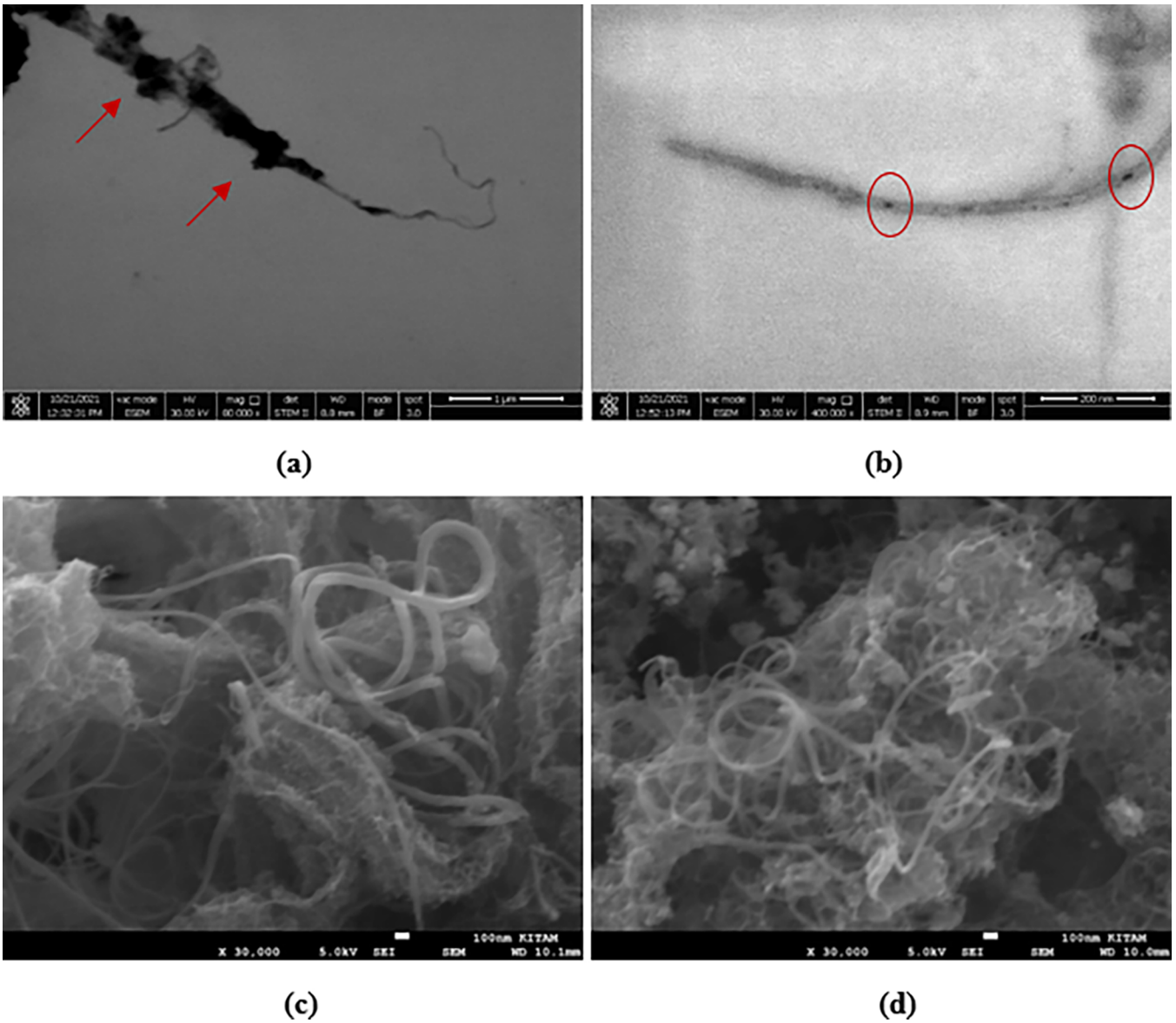

Figure 3. (a, b) FEG-SEM images of synthesized mCNT and SEM images of (c) carboxylated CNT and (d) mCNT.

was observed for both samples (Figure S4), which proves that the particle size of the CNTs is less than 2 nm.

The crystal structure of the synthesized CNT and mCNT was determined by XRD analysis. As seen from Figure 2,

https://doi.org/10.1021/acsomega.3c09608
ACS Omega 2025, 10, 102−113

characteristic peaks for CNT that are seen at 2θ = 26.13 and 43.40° positions can be associated with the (002) and (100) planes, respectively.[53] The main peaks of the cubic spinel structure of the Fe_3O_4 crystal are seen in the XRD pattern of mCNT. Accordingly, the characteristic diffraction peaks of magnetite appeared at 2θ of 30.12, 35.63, 43.23, 53.98, 57.11, and 62.95° corresponding to the (220), (311), (400), (422), (511), and (440) planes, respectively.[54] The XRD pattern of mCNT represents the diffraction peak of CNT (002), indicating the successful synthesis of magnetic carbon nanotubes. Our results are compatible with the previous studies.[55−58]

Synthesized mCNT was characterized by FEG-SEM as shown in Figure 3a,b. After the carbon nanotubes were synthesized, they were purified with HNO_3 and this treatment allowed the formation of −COOH groups on the surface of the CNTs. The black parts (marked as red) in Figure 3a represent Fe_3O_4 nanoparticles, and MNPs can be present in high concentrations in some regions where −COOH groups are intense. It is clear that iron oxide nanoparticles attached to CNT. Carboxylated CNT and mCNT were also characterized by SEM as shown in Figure 3c,d, respectively. The SEM images obviously depict that the synthesized CNTs have a tubular shape and are in nanometric size range. CNTs have a spaghetti form and a nanoneedle-like structure (Figure 3c).[59] As can be seen from Figure 3d, no changes in the morphology of mCNTs are determined.

As depicted in Table 2, EDS analysis confirmed that only C, O, and Fe are present in the synthesized CNT and mCNT, and

Table 2. SEM-EDS Results of Carboxylated CNT and mCNT

sample	C (%)	O (%)	Fe (%)	total
carboxylated CNT	84.55	14.84	0.61	100.00
mCNT	68.14	16.37	15.49	100.00

no other elements were detected. It is seen that the carboxylated CNT contains the iron element (0.61%) originating from the catalyst used during the synthesis. According to purification studies on CNT, nitric acid provides high oxidation efficiency, while it cannot achieve catalyst removal completely.[13,60] Furthermore, EDS measurements of mCNT demonstrate the presence of C (68.14%), O (16.37%), and Fe (15.49%) in the mCNTs and an increase in atomic percentage of Fe indicated that the preparation of magnetic carbon nanotubes is successful.

Considering the TGA curves of the nanocarriers in the oxygen environment, the residual mass amounts were calculated as 2.5 and 32.8% for CNT and mCNT, respectively (Figure S5). TGA results are in good agreement with the SEM-EDS results. The TGA results reported by Yang et al.,[61] in which the same ratio of CNT to Fe_3O_4 (2/1 wt) was prepared, also support these results. Moreover, the TGA curves demonstrate that the maximal weight loss occurs at 585 and 540 °C for CNT and mCNT, respectively, due to the catalytic effect of metal oxides.[53]

The XPS technique was also used to obtain information about functional groups on the nanotube surface. As depicted in Figure 4a, the peaks at 284, 532, and 711 eV can be ascribed to C 1s, O 1s, and Fe 2p, respectively. Figure 4b shows the Fe 2p spectrum of mCNT. The peaks at 711 and 725 eV can be assigned to Fe $2p_{3/2}$ and Fe $2p_{1/2}$, respectively, which indicates the presence of Fe_3O_4.[54,57,61,62] As seen from Figure 4c, the C 1s peaks can be deconvoluted C−C/C═O at 284.1 eV, CH_2 at 285.3 eV, and HO−C═O at 288.6 eV.[60,63] The deconvolution analysis of O 1s (Figure 4d) shows two components in spectra associated with peaks at 530.5 and 532.0 eV corresponding to Fe−O and −C−O/−C═O bonds, respectively.[50,61]

FT-IR spectroscopy (Figure S6 and Table S1) and XPS analysis confirmed the presence of −COOH in the structure of CNTs, and the −COOH contents also were determined by titration. An acid−base titration method was evaluated to specify the concentration of −COOH groups on the surface of CNT by the method reported.[50] −COOH contents of carboxylated CNT and mCNT were found to be 17.53 ± 2.13 and 10.35 ± 4.04 mmol/g, respectively (Figure 5). Accordingly, it was determined that there was a decrease in the amount of −COOH after Fe_3O_4 nanoparticles were added to the CNT.

Characterization of BSA-Coated mCNTs. FT-IR spectroscopy was used to check functional groups in the nanocarrier structure. The FT-IR spectra of mCNT, BSA, and mCNT-BSA conjugates are shown in Figure 6. To prove the covalent attachment of BSA to mCNT, a blank experiment was also done in which mCNT was modified with BSA without EDC/NHS by a noncovalent method. Other parameters were kept constant. It was considered as the control group to compare with FT-IR and Raman spectra of mCNT-BSA. The characteristic peaks of BSA at 1646 and 1532 cm^{-1} were dedicated to vibration of amide I (C═O) and amide II (N−H and C−N), respectively.[64] After BSA binding onto mCNT surfaces by covalent modification, a slight shift occurs in the amide I and II band positions for mCNT-BSA to 1643 and 1533 cm^{-1}, respectively.[52] The new peaks at 1020 cm^{-1} (C−N) and 1730 cm^{-1} (N−H) were observed, which represented the new amide bond of mCNT-BSA.[52,65] mCNT modified with BSA by a noncovalent method exhibited only two obvious peaks at 1646 and 1535 cm^{-1}, corresponding to amide I and amide II, respectively. As depicted in Figure 6, all of the characteristic peaks of mCNT and BSA could be present in the FT-IR spectra of mCNT-BSA. These results indicated successful covalent functionalization of mCNT with BSA.

Raman spectra of pristine and BSA-coated mCNTs are presented in Figure 7. The I_D/I_G ratio can be used to obtain information about structural changes as a consequence of functionalization. The I_D/I_G ratios for BSA-coated nanocarriers increased to 0.53 and 0.82 for noncovalent and covalent binding carriers, respectively. Covalent functionalization produces considerably more defects on the surface of the CNTs and would have markedly increased the I_D/I_G ratios in comparison with noncovalent functionalization.[66,67] At the same time, as seen from Figure 7, the graphitic structure of CNTs is still protected since the G band is present in the spectra for all nanotubes.

TGA was used to determine the content of BSA attached to mCNT. As observed in Figure 8, nanocarriers have weight losses until 1000 °C, which are attributed to the volatilization of adsorbed water. The weight loss of mCNT-BSA was 28.2%, while mCNT and BSA had 14.9 and 86.0% weight loss at 1000 °C in a nitrogen atmosphere, respectively. The mCNT-BSA presented additional 13.3% weight loss, which was caused by an increase in organic content of the nanoparticle.[68] Furthermore, weight losses in coated mCNT mainly occurred between 200 and 400 °C, and these results confirm the attachment of BSA to the mCNT.

In addition to the characterization described above, the surface elemental composition of CNTs was also investigated by XPS. Figure 9a shows the wide scan spectrum of mCNT-BSA. The results indicated that mCNT-BSA mainly contained Fe, O, C, N, and S elements. BSA contains the nitrogen and sulfur

https://doi.org/10.1021/acsomega.3c09608
ACS Omega 2025, 10, 102−113

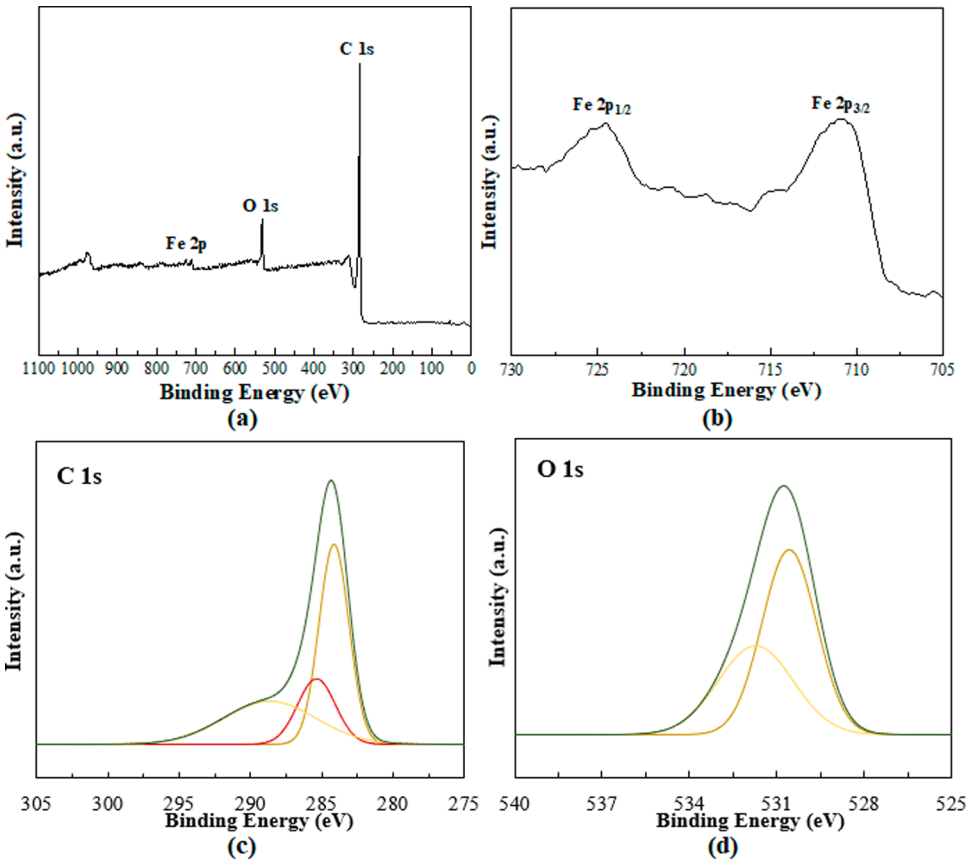

Figure 4. XPS spectra of mCNT: (a) wide scan, (b) Fe 2p, (c) C 1s, and (d) O 1s.

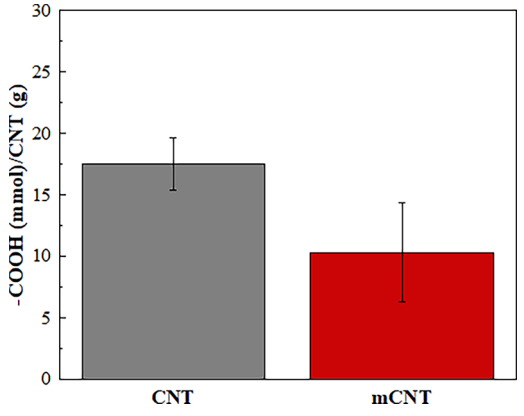

Figure 5. −COOH contents of CNT and mCNT.

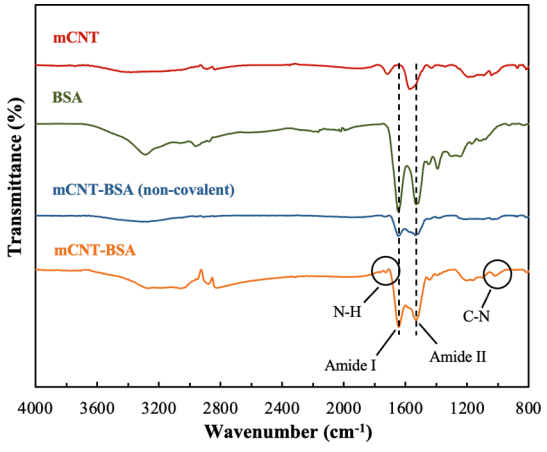

Figure 6. FT-IR spectra of mCNT, BSA, and BSA-coated mCNTs.

elements, but mCNT does not. The XPS results demonstrated the BSA has been successfully grafted onto the surface of mCNT. The XPS spectrum of N 1s is shown in Figure 9b. The binding energies of amine (NH_2) and amide (N−C═O) are seen at 399 and 401 eV, respectively. This confirmed that BSA has been successfully linked to the mCNT surface using covalent functionalization.[69]

The mCNT-BSA was characterized with SEM analysis (Figure 10). mCNT-BSA did not exhibit morphology changes compared to mCNT. The image of mCNT-BSA suggests that there was no change in the CNT structure after BSA conjugation. Red marking was used to indicate BSA in the SEM image.

The magnetic properties of synthesized nanomaterials were investigated by VSM (Figure 11). S-like magnetization curves at room temperature without remanence and coercivity usually represent the superparamagnetic behavior of all nanomaterials.[8] Generally, this feature allows for easy separation of the magnetic nanomaterials from the mixture using an external magnetic field. Once the external magnetic field has been removed, nanomaterials can be redispersed by gentle shaking, which is essential for their applications in the biological field.[62,70,71] The curve shows that the saturation magnetization (M_s) of mCNT is about 16.8 emu/g, which is much lower than that of bulk Fe_3O_4 (41.3 emu/g). This result is attributed to magnetic CNT being successfully prepared by the ligand exchange method. After being coated with nonmagnetic BSA, the saturation magnetization of the mCNT was reduced to 15.6 emu/g because of the quenching of

https://doi.org/10.1021/acsomega.3c09608
ACS Omega 2025, 10, 102−113

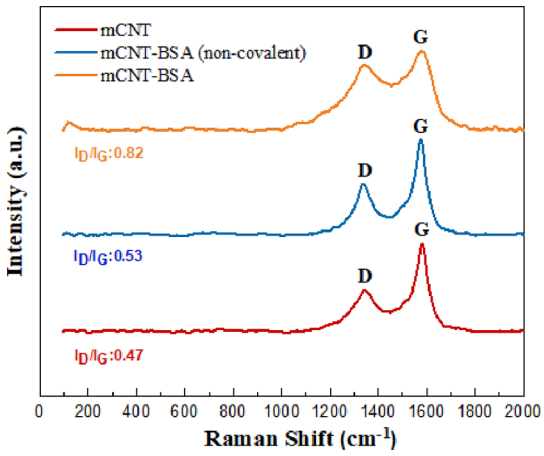

Figure 7. Raman spectra of mCNT, noncovalent functionalized mCNT-BSA, and mCNT-BSA.

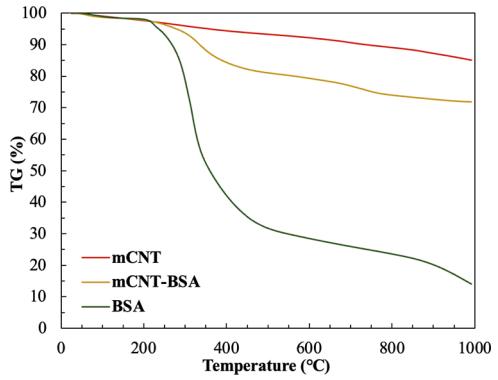

Figure 8. TGA curves of mCNT, mCNT-BSA, and BSA.

surface moments. Previous studies have reported magnetization values of nanocarriers prepared as drug carrier systems. Multiwalled CNT/Fe_3O_4 conjugates were prepared by Ghoderao et al.[14] for doxycycline delivery. The M_s value of the nanocarrier was reported as 13.4 emu/g. In another study, Suo et al.[11] demonstrated an epirubicin-loaded magnetic multiwalled CNT system, and the M_s value of magnetic CNT was found to be 19.13 emu/g. The measured M_s values in this study are compatible with the ones reported in the literature.

MTO Loading and Release. The MTO loading and release contents of mCNT and mCNT-BSA were determined by UV–vis spectroscopy (Figure 12). The drug loading efficiency for mCNT was found to be 78.8%. Compared with mCNT, the loading efficiency of MTO in mCNT-BSA was lower with the loading efficiency of 43.4%. The drug contents for mCNT and mCNT-BSA conjugates were found to be 263 and 145 μg/mg, respectively. After covalent coating with BSA, the MTO loading efficiency and loading capacity of mCNT were decreased due to weakening of $\pi-\pi$ interactions between mCNT and MTO molecules.

The release of MTO from mCNT and mCNT-BSA at different pH values (5.5 and 7.4) is shown in Figure 13. It has a sustained pattern followed after initial burst release for the first 6 h. As depicted in Figure 13, mCNT clearly exhibited pH-dependent MTO release. Only 0.142 mg (22.71%) of the loaded MTO was released from mCNT after 120 h at pH 7.4, while 0.183 mg (29.45%) of the loaded MTO molecules was released from mCNT at pH 5.5. Because amine groups of MTO molecules were protonated and the hydrophobic interactions between MTO molecules and the mCNT were decreased in an acidic medium, this accelerated the MTO release.

In contrast, the MTO loading of mCNT-BSA is lower and its release is faster than that of mCNT. The faster drug release accounted for more hydrophilicity and cleavage of $\pi-\pi$ interaction between the MTO molecule and mCNT. Since BSA is an additional shell for the drug, it can lead to weakening of the interactions between MTO and mCNT. The release behavior of mCNT-BSA after 120 h at different pH values was very similar (0.174 vs 0.165 mg and 43.6 vs 45.71%). Regarding MTO release results from nanocarriers, mCNT-MTO is unsuitable for biomedical application due to the short half-time of Fe_3O_4 nanoparticles in the human body. On the contrary, the mCNT-BSA has a good potential for active targeting, and the selectivity of mCNT-BSA can be increased using ligands such as folic acid.

Finally, zero-order, first-order, Higuchi, and Korsmeyer-Peppas model equations were employed to evaluate MTO release kinetics from mCNT and mCNT-BSA nanocarriers. The results indicated that the equations are not valid for all release stages, in particular, after the first 24 h. For this reason, we investigated the MTO release mechanism from nanocarriers between 0 and 24 h. The best fit was obtained from the Korsmeyer–Peppas equation. The n value obtained for all

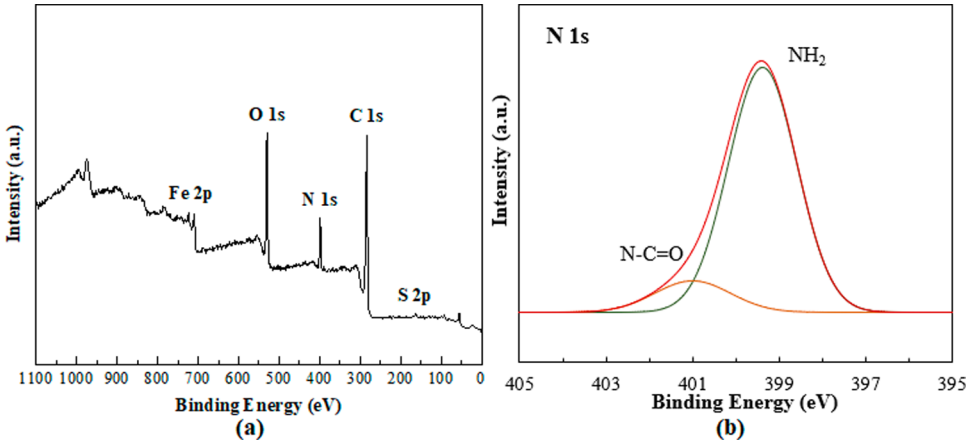

Figure 9. XPS spectra of mCNT-BSA: (a) wide scan and (b) N 1s.

https://doi.org/10.1021/acsomega.3c09608
ACS Omega 2025, 10, 102−113

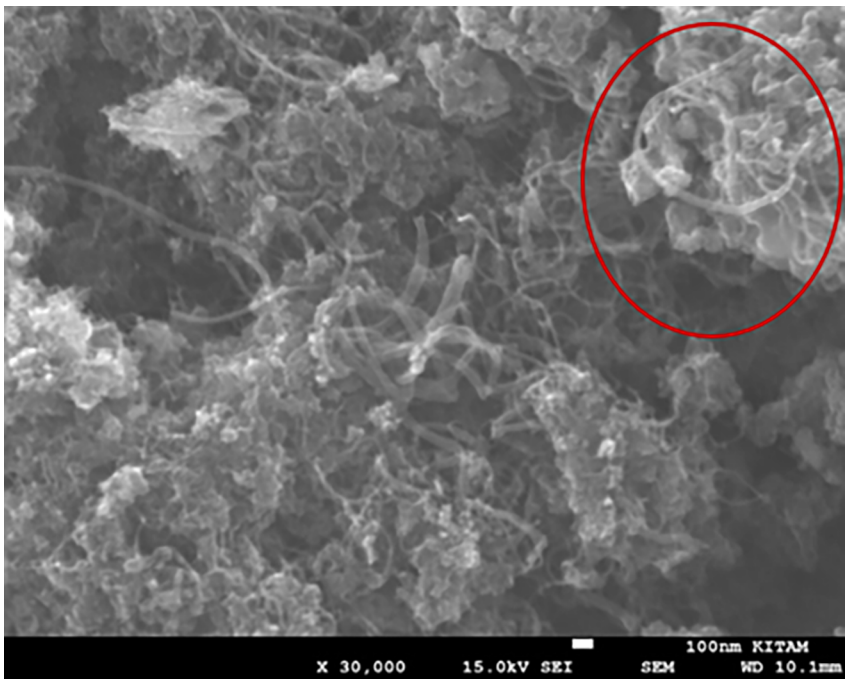

Figure 10. SEM image of mCNT-BSA.

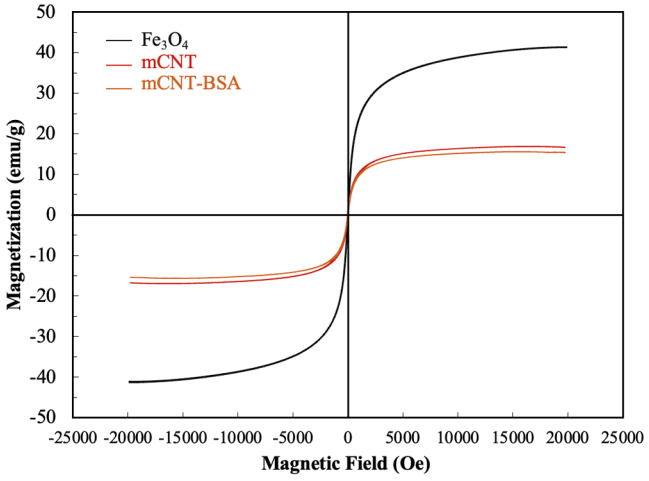

Figure 11. Magnetization curves of Fe_3O_4, mCNT, and mCNT-BSA.

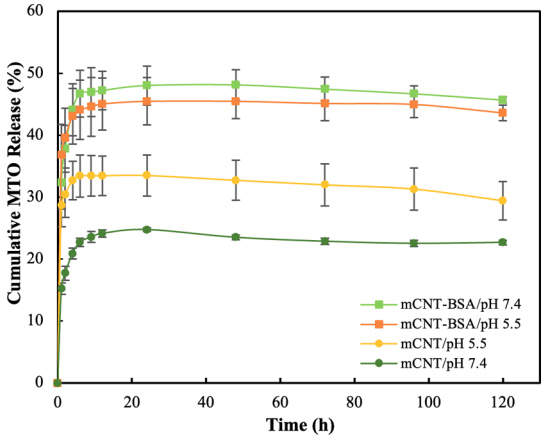

Figure 13. Cumulative MTO release from mCNT and mCNT-BSA at 37 °C in PBS.

nanocarriers was smaller than 0.45 (Table S2). Therefore, Fickian diffusion is the main drug release mechanism.[72,73] In addition, the k_P values of nanocarriers at pH 5.5 were much higher than those of 7.4, indicating the higher release rate at pH 5.5.[74]

In Vitro Cytotoxicity Assay. Functionalizing magnetic CNTs with BSA can prolong the residence time of the nanocarriers in the body. For this reason, the cytotoxic effects

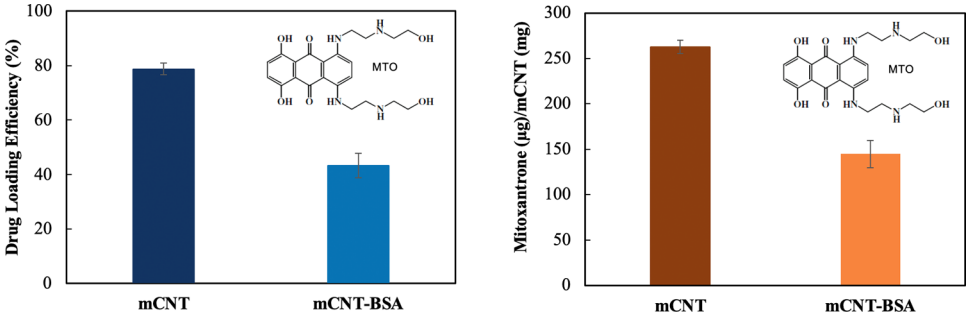

Figure 12. Drug loading efficiencies and contents of mCNT and mCNT-BSA.

https://doi.org/10.1021/acsomega.3c09608
ACS Omega 2025, 10, 102−113

of nanocarriers were employed using an MTT assay on HEK293T and MDA-MB-231 cell lines. HEK293T was treated with Fe_3O_4, CNT, mCNT, and mCNT-BSA at different concentrations of 5, 10, 25, and 50 μg/mL. The untreated cells are used as a control. As shown in Figure 14, no significant cytotoxicity was observed for Fe_3O_4 even at 50 μg/mL concentration. Fe_3O_4 showed the best distribution in the solution media compared with other nanocarriers.

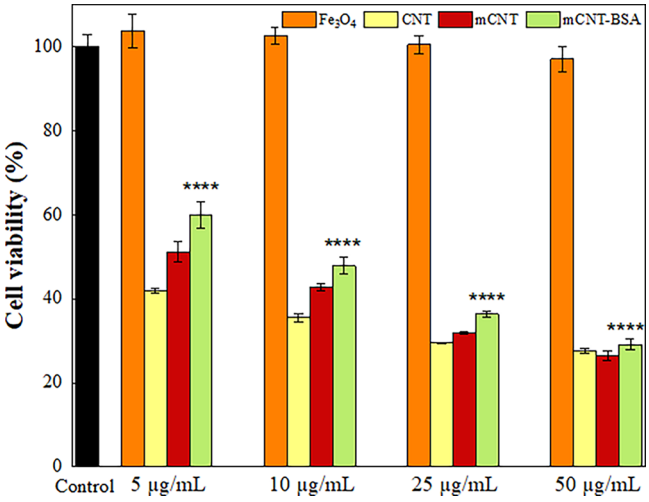

Figure 14. Cell viability results for nanocarriers on HEK293T cells by the MTT assay. Data are represented as the mean ± SD (n = 3). One-way analysis of variance (ANOVA) with Tukey posthoc test; ****p < 0.0001 compared to the control.

On the other hand, CNT has significant toxicity on the cell line at all applied concentrations. This result highlights why functionalization of mCNTs is essential. It was found that cell viability slightly decreased with an increase in the concentration of nanoparticles. The cell viability of BSA-coated mCNT is higher than that of mCNT at a concentration of 5 μg/mL. This result showed that modification with biocompatible BSA decreased the toxicity of mCNTs. Also, statistical analysis (Tukey's multiple comparisons test) results revealed a significant difference in cell viability between all nanoparticle groups (except Fe_3O_4) and control groups (p < 0.05) after 48 h.

Cell studies of MTO-free mCNT and mCNT-BSA at concentrations of 5 and 25 μg/mL were also performed as a blank on MDA-MB-231 (Figure 15). It has been determined that increasing the concentration of nanocarriers from 5 to 25 μg/mL creates more cytotoxicity in the cell line (p < 0.05). Furthermore, the cell viability (%) of the mCNT-BSA increased compared to mCNT (p < 0.05).

Figure 16a depicts the cell viability of free MTO and MTO-loaded nanocarriers at concentrations of 5 and 25 μg/mL. As expected, cell viability values decreased as the nanocarrier concentration increased from 5 to 25 μg/mL due to the increased concentration of MTO to which the cells were exposed. The viability of the MDA-MB-231 cells increased from 36.41 to 60.06% at a 5 μg/mL concentration after mCNT was coated with BSA.

After 48 h treatment, the cell viability (%) for mCNT/MTO and mCNT-BSA/MTO is higher than that of free MTO at the same MTO concentration (p < 0.05). Moreover, it is seen that the critical cytotoxicity was caused by MTO released from nanocarriers. The free drug interacts directly with the cells fast

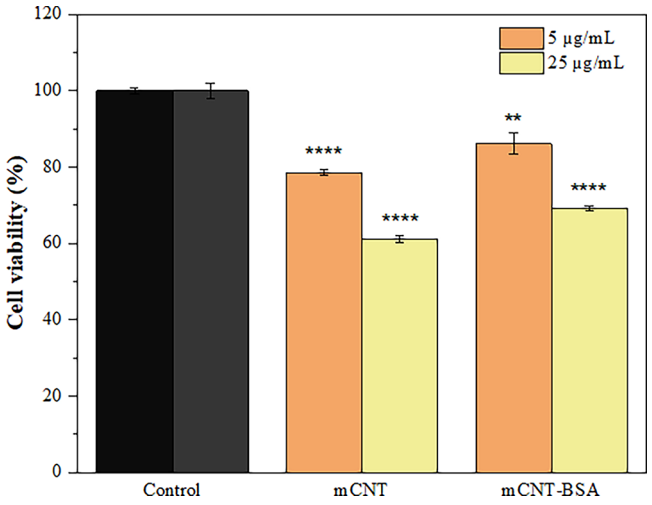

Figure 15. Cell viability results for mCNT and mCNT-BSA on MDA-MB-231 cells. Data are represented as the mean ± SD (n = 3). One-way analysis of variance (ANOVA) with Tukey posthoc test; **p < 0.01 and ****p < 0.0001 compared to the control.

via diffusion and may also be harmful to healthy tissues and cells, limiting chemotherapeutic agent clinical applications. However, drugs are partially released from the nanocarriers at the targeted site before interacting with the cells, so its cytotoxicity is reduced. mCNT-BSA is a nanosized carrier, which may anticipate advantages, such as increased drug accumulation in cancerous tissues and less cytotoxic effect on healthy cells due to the slow release of drugs from the nanocarriers. While free MTO leads to a higher cytotoxic effect, mCNT-BSA can be the best choice and be used as a promising drug delivery system to enhance the therapeutic efficacy of MTO.

No significant difference was obtained in the cell studies conducted with magnet treatment (Figure 16b) compared to those without magnetic treatment (p > 0.05). The temperature increase at this concentration may not have caused a significant difference in drug release. However, the magnetic property of the nanocarrier is fundamental in reducing the toxic effect on healthy cells.

CONCLUSIONS

In this study, mCNT-BSA was successfully prepared using EDC/NHS as a magnetic targeted drug delivery carrier for the controllable release of MTO. FT-IR spectroscopy, SEM, XPS, and Raman spectroscopy are used to confirm the attachment of BSA on the mCNT. The new peaks at 1020 and 1730 cm^{-1} in the FT-IR spectra of mCNT-BSA indicated C−N and N−H bonds between mCNT and BSA, respectively. After covalent functionalization, the I_D/I_G ratio for mCNT increased from 0.47 to 0.82. XPS analysis showed that mCNT-BSA contains nitrogen and sulfur elements as well as iron, oxygen, and carbon. BSA conjugation of mCNT decreased the drug loading from 78.8 to 43.4% but increased the MTO release (%). The decrease in loading and the increase in release contributed to the enhanced hydrophilicity by BSA conjugation onto the surface of mCNT. The magnetic saturation value of the mCNT-BSA is 15.6 emu/g, and the novel carrier exhibits suitable superparamagnetic property at room temperature. Modification with biocompatible BSA decreased the toxicity of mCNTs. Furthermore, cell viability (%) is significantly reduced with MTO-loaded mCNT and mCNT-BSA, and it is higher than that

https://doi.org/10.1021/acsomega.3c09608
ACS Omega 2025, 10, 102−113

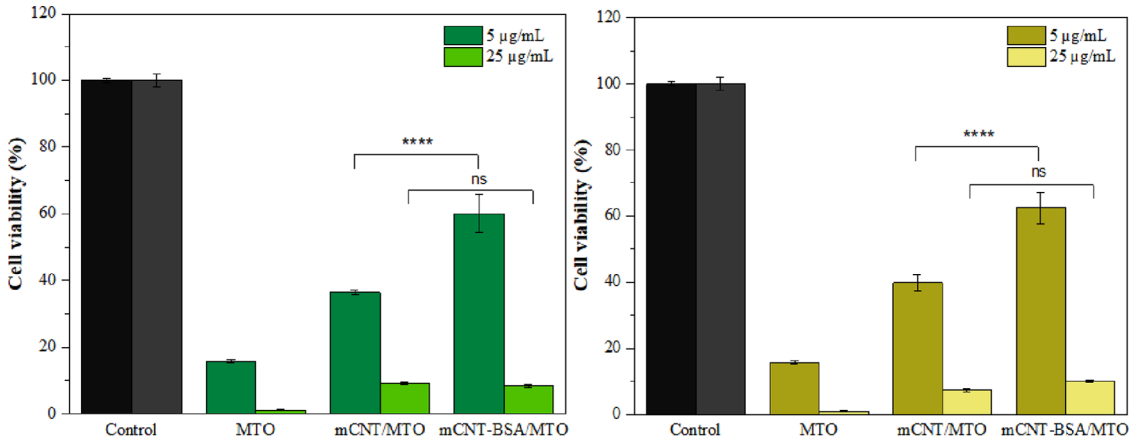

Figure 16. Cell viability results for free MTO and MTO-loaded nanocarriers at concentrations of 5 and 25 μg/mL on MDA-MB-231 (a) without and (b) with a magnet. Data are represented as the mean ± SD (n = 3). One-way analysis of variance (ANOVA) with Tukey posthoc test; ns indicates not significant and ****p < 0.0001 for mCNT/MTO vs mCNT-BSA/MTO.

of free MTO. Results demonstrate that mCNT-BSA/MTO may be a proper delivery system for cancer treatment.

■ ASSOCIATED CONTENT

Supporting Information

The Supporting Information is available free of charge at https://pubs.acs.org/doi/10.1021/acsomega.3c09608.

Calibration curves for MTO at pH 9 (Figure S1), pH 5.5 (Figure S2), and pH 7.4 (Figure S3); Raman spectra (Figure S4); TGA curves in air atmosphere (Figure S5); FT-IR spectra for CNT and mCNT (Figure S6); FT-IR results of mCNT (Table S1); kinetic model data for nanocarriers (Table S2) (PDF)

■ AUTHOR INFORMATION

Corresponding Author

F. Seniha Güner − *Department of Chemical Engineering, Istanbul Technical University, Istanbul 34469, Türkiye; Sabancı University Nanotechnology Research and Application Center (SUNUM), Istanbul 34956, Türkiye;* orcid.org/0000-0002-3414-4868; Email: seniha.guner@sabanciuniv.edu

Authors

Buğçe Aydın − *Department of Chemical Engineering, Istanbul Technical University, Istanbul 34469, Türkiye; Department of Chemical Engineering, Ondokuz Mayıs University, Samsun 55139, Türkiye;* orcid.org/0000-0001-5104-1484

Serdar Bozoğlu − *Energy Institute, Renewable Energy Division, Istanbul Technical University, Istanbul 34469, Türkiye*

Nilgün Karatepe − *Energy Institute, Renewable Energy Division, Istanbul Technical University, Istanbul 34469, Türkiye*

Complete contact information is available at: https://pubs.acs.org/10.1021/acsomega.3c09608

Author Contributions

All authors have given approval to the final version of the manuscript.

Notes

The authors declare no competing financial interest.

■ ACKNOWLEDGMENTS

This work was supported by Istanbul Technical University Scientific Research Project Foundation (MDK-2020-42751).

■ REFERENCES

(1) Tran, S.; DeGiovanni, P.; Piel, B.; Rai, P. Cancer Nanomedicine: A Review of Recent Success in Drug Delivery. *Clin. Transl. Med.* **2017**, *6* (1), 44.

(2) Mahajan, S.; Patharkar, A.; Kuche, K.; Maheshwari, R.; Deb, P. K.; Kalia, K.; Tekade, R. K. Functionalized Carbon Nanotubes as Emerging Delivery System for the Treatment of Cancer. *Int. J. Pharm.* **2018**, *548* (1), 540−558.

(3) Sheikhpour, M.; Golbabaie, A.; Kasaeian, A. Carbon Nanotubes: A Review of Novel Strategies for Cancer Diagnosis and Treatment. *Mater. Sci. Eng., C* **2017**, *76*, 1289−1304.

(4) Liyanage, P. Y.; Hettiarachchi, S. D.; Zhou, Y.; Ouhtit, A.; Seven, E. S.; Oztan, C. Y.; Celik, E.; Leblanc, R. M. Nanoparticle-Mediated Targeted Drug Delivery for Breast Cancer Treatment. *Biochim. Biophys. Acta - Rev. Cancer* **2019**, *1871* (2), 419−433.

(5) Unsoy, G.; Khodadust, R.; Yalcin, S.; Mutlu, P.; Gunduz, U. Synthesis of Doxorubicin Loaded Magnetic Chitosan Nanoparticles for pH Responsive Targeted Drug Delivery. *Eur. J. Pharm. Sci.* **2014**, *62*, 243−250.

(6) Gawali, S. L.; Shelar, S. B.; Gupta, J.; Barick, K. C.; Hassan, P. A. Immobilization of Protein on Fe_3O_4 Nanoparticles for Magnetic Hyperthermia Application. *Int. J. Biol. Macromol.* **2021**, *166*, 851−860.

(7) Zuo, X.; Wu, C.; Zhang, W.; Gao, W. Magnetic Carbon Nanotubes for Self-Regulating Temperature Hyperthermia. *RSC Adv.* **2018**, *8* (22), 11997−12003.

(8) De Santana, W. M. O. S.; Abramson, S.; Fini, R.; Caetano, B. L.; Ménager, C.; Pulcinelli, S. H.; Santilli, C. V. Ureasil-Polyether-$CoFe_2O_4$ Nanocomposites: Coupling a Drug Delivery System and Magnetic Hyperthermia. *ACS Appl. Polym. Mater.* **2021**, *3* (10), 4837−4848.

(9) Sumitha, N. S.; Krishna, N. G.; Sailaja, G. S. Multifunctional Chitosan Ferrogels for Targeted Cancer Therapy by On-Demand Magnetically Triggered Drug Delivery and Hyperthermia. *Biomater. Adv.* **2022**, *142*, No. 213137.

(10) Huang, Y.-S.; Lu, Y.-J.; Chen, J.-P. Magnetic Graphene Oxide as a Carrier for Targeted Delivery of Chemotherapy Drugs in Cancer Therapy. *J. Magn. Magn. Mater.* **2017**, *427*, 34−40.

(11) Suo, N.; Wang, M.; Jin, Y.; Ding, J.; Gao, X.; Sun, X.; Zhang, H.; Cui, M.; Zheng, J.; Li, N.; Jin, X.; Jiang, S. Magnetic Multiwalled Carbon Nanotubes with Controlled Release of Epirubicin: An Intravesical Instillation System for Bladder Cancer. *Int. J. Nanomedicine* **2019**, *14*, 1241−1254.

(12) Wang, D.; Li, X.; Li, X.; Kang, A.; Sun, L.; Sun, M.; Yang, F.; Xu, C. Magnetic and PH Dual-Responsive Nanoparticles for Synergistic Drug-Resistant Breast Cancer Chemo/Photodynamic Therapy. *Int. J. Nanomedicine* **2019**, *14*, 7665−7679.
(13) Li, H.; Sun, X.; Li, Y.; Li, B.; Liang, C.; Wang, H. Preparation and Properties of Carbon Nanotube (Fe)/Hydroxyapatite Composite as Magnetic Targeted Drug Delivery Carrier. *Mater. Sci. Eng., C* **2019**, *97*, 222−229.
(14) Ghoderao, P.; Sahare, S.; Alegaonkar, P.; Kulkarni, A. A.; Bhave, T. Multiwalled Carbon Nanotubes Decorated with Fe_3O_4 Nanoparticles for Efficacious Doxycycline Delivery. *ACS Appl. Nano Mater.* **2019**, *2* (1), 607−616.
(15) Hwang, Y.; Park, S.-H.; Lee, J. Applications of Functionalized Carbon Nanotubes for the Therapy and Diagnosis of Cancer. *Polymers* **2017**, *9* (1), 13.
(16) Hosnedlova, B.; Kepinska, M.; Fernandez, C.; Peng, Q.; Ruttkay-Nedecky, B.; Milnerowicz, H.; Kizek, R. Carbon Nanomaterials for Targeted Cancer Therapy Drugs: A Critical Review. *Chem. Rec.* **2019**, *19* (2), 502−522.
(17) Tian, Z.; Shi, Y.; Yin, M.; Shen, H.; Jia, N. Functionalized Multiwalled Carbon Nanotubesanticancer Drug Carriers: Synthesis, Targeting Ability and Antitumor activity. *Nano Biomed. Eng.* **2011**, *3*, 157−162.
(18) Yu, B.; Tan, L.; Zheng, R.; Tan, H.; Zheng, L. Targeted Delivery and Controlled Release of Paclitaxel for the Treatment of Lung Cancer Using Single-Walled Carbon Nanotubes. *Mater. Sci. Eng., C* **2016**, *68*, 579−584.
(19) Huang, H.; Yuan, Q.; Shah, J. S.; Misra, R. D. K. A New Family of Folate-Decorated and Carbon Nanotube-Mediated Drug Delivery System: Synthesis and Drug Delivery Response. *Adv. Drug Delivery Rev.* **2011**, *63* (14−15), 1332−1339.
(20) Singh, R. P.; Sharma, G.; Sonali; Singh, S.; Bharti, S.; Pandey, B. L.; Koch, B.; Muthu, M. S. Chitosan-Folate Decorated Carbon Nanotubes for Site Specific Lung Cancer Delivery. *Mater. Sci. Eng., C* **2017**, *77*, 446−458.
(21) Dinan, N. M.; Atyabi, F.; Rouini, M. R.; Amini, M.; Golabchifar, A. A.; Dinarvand, R. Doxorubicin Loaded Folate-Targeted Carbon Nanotubes: Preparation, Cellular Internalization, in Vitro Cytotoxicity and Disposition Kinetic Study in the Isolated Perfused Rat Liver. *Mater. Sci. Eng., C* **2014**, *39* (1), 47−55.
(22) Razzazan, A.; Atyabi, F.; Kazemi, B.; Dinarvand, R. In Vivo Drug Delivery of Gemcitabine with PEGylated Single-Walled Carbon Nanotubes. *Mater. Sci. Eng., C* **2016**, *62*, 614−625.
(23) Heister, E.; Neves, V.; Lamprecht, C.; Silva, S. R. P.; Coley, H. M.; McFadden, J. Drug Loading, Dispersion Stability, and Therapeutic Efficacy in Targeted Drug Delivery with Carbon Nanotubes. *Carbon N. Y.* **2012**, *50* (2), 622−632.
(24) Heister, E.; Neves, V.; Tîlmaciu, C.; Lipert, K.; Beltrán, V. S.; Coley, H. M.; Silva, S. R. P.; McFadden, J. Triple Functionalisation of Single-Walled Carbon Nanotubes with Doxorubicin, a Monoclonal Antibody, and a Fluorescent Marker for Targeted Cancer Therapy. *Carbon N. Y.* **2009**, *47* (9), 2152−2160.
(25) Habibizadeh, M.; Rostamizadeh, K.; Dalali, N.; Ramazani, A. Preparation and Characterization of PEGylated Multiwall Carbon Nanotubes as Covalently Conjugated and Non-Covalent Drug Carrier: A Comparative Study. *Mater. Sci. Eng., C* **2017**, *74*, 1−9.
(26) Mehra, N. K.; Palakurthi, S. Interactions between Carbon Nanotubes and Bioactives: A Drug Delivery Perspective. *Drug Discovery Today* **2016**, *21* (4), 585−597.
(27) Chen, Z.; Zhang, A.; Wang, X.; Zhu, J.; Fan, Y.; Yu, H.; Yang, Z.The Advances of Carbon Nanotubes in Cancer Diagnostics and Therapeutics. *J. Nanomater.***2017**, *2017*. 1.
(28) Zhao, D.; Zhao, X.; Zu, Y.; Li, J.; Zhang, Y.; Jiang, R.; Zhang, Z. Preparation, Characterization, and in Vitro Targeted Delivery of Folate-Decorated Paclitaxel-Loaded Bovine Serum Albumin Nanoparticles. *Int. J. Nanomed.* **2010**, *5* (1), 669−677.
(29) Xiong, K.; Fan, Q.; Wu, T.; Shi, H.; Chen, L.; Yan, M. Enhanced Bovine Serum Albumin Absorption on the N-Hydroxysuccinimide Activated Graphene Oxide and Its Corresponding Cell Affinity. *Mater. Sci. Eng.: C* **2017**, *81*, 386−392.
(30) Salehiabar, M.; Nosrati, H.; Javani, E.; Aliakbarzadeh, F.; Kheiri Manjili, H.; Davaran, S.; Danafar, H. Production of Biological Nanoparticles from Bovine Serum Albumin as Controlled Release Carrier for Curcumin Delivery. *Int. J. Biol. Macromol.* **2018**, *115*, 83−89.
(31) Van de Sande, L.; Cosyns, S.; Willaert, W.; Ceelen, W. Albumin-Based Cancer Therapeutics for Intraperitoneal Drug Delivery: A Review. *Drug Delivery* **2020**, *27* (1), 40−53.
(32) Tian, R.; Long, X.; Yang, Z.; Lu, N.; Peng, Y.-Y. Formation of a Bovine Serum Albumin Diligand Complex with Rutin and Single-Walled Carbon Nanotubes for the Reduction of Cytotoxicity. *Biophys. Chem.* **2020**, *256*, No. 106268.
(33) Iqbal, H.; Razzaq, A.; Khan, N. U.; Rehman, S. U.; Webster, T. J.; Xiao, R.; Menaa, F. PH-Responsive Albumin-Coated Biopolymeric Nanoparticles with Lapatinab for Targeted Breast Cancer Therapy. *Biomater. Adv.* **2022**, *139* (May), No. 213039.
(34) Barar, J.; Kafil, V.; Majd, M. H.; Barzegari, A.; Khani, S.; Johari-Ahar, M.; Asgari, D.; Cokous, G.; Omidi, Y. Multifunctional Mitoxantrone-Conjugated Magnetic Nanosystem for Targeted Therapy of Folate Receptor-Overexpressing Malignant Cells. *J. Nanobiotechnology* **2015**, *13* (1), 1−16.
(35) Khan, S. N.; Islam, B.; Yennamalli, R.; Sultan, A.; Subbarao, N.; Khan, A. U. Interaction of Mitoxantrone with Human Serum Albumin: Spectroscopic and Molecular Modeling Studies. *Eur. J. Pharm. Sci.* **2008**, *35* (5), 371−382.
(36) Hande, K. R. Topoisomerase II Inhibitors. *Update Cancer Ther.* **2008**, *3* (1), 13−26.
(37) Enache, M.; Toader, A.; Enache, M. I. Mitoxantrone-Surfactant Interactions: A Physicochemical Overview. *Molecules* **2016**, *21* (10), 1356.
(38) Risi, G.; Bloise, N.; Merli, D.; Icaro-Cornaglia, A.; Profumo, A.; Fagnoni, M.; Quartarone, E.; Imbriani, M.; Visai, L. Invitro Study of Multiwall Carbon Nanotubes (MWCNTs) with Adsorbed Mitoxantrone (MTO) as a Drug Delivery System to Treat Breast Cancer. *RSC Adv.* **2014**, *4* (36), 18683−18693.
(39) Zaloga, J.; Feoktystov, A.; Garamus, V. M.; Karawacka, W.; Ioffe, A.; Brückel, T.; Tietze, R.; Alexiou, C.; Lyer, S. Studies on the Adsorption and Desorption of Mitoxantrone to Lauric Acid/Albumin Coated Iron Oxide Nanoparticles. *Colloids Surfaces B Biointerfaces* **2018**, *161*, 18−26.
(40) Hou, L.; Feng, Q.; Wang, Y.; Yang, X.; Ren, J.; Shi, Y.; Shan, X.; Yuan, Y.; Wang, Y.; Zhang, Z. Multifunctional Hyaluronic Acid Modified Graphene Oxide Loaded with Mitoxantrone for Overcoming Drug Resistance in Cancer. *Nanotechnology* **2015**, *27* (1), No. 15701.
(41) Wani, A.; Savithra, G. H. L.; Abyad, A.; Kanvinde, S.; Li, J.; Brock, S.; Oupický, D. Surface PEGylation of Mesoporous Silica Nanorods (MSNR): Effect on Loading, Release, and Delivery of Mitoxantrone in Hypoxic Cancer Cells. *Sci. Rep.* **2017**, *7* (1), 1−11.
(42) Sargazi, A.; Shiri, F.; Keikha, S.; Majd, M. H. Hyaluronan Magnetic Nanoparticle for Mitoxantrone Delivery toward CD44-Positive Cancer Cells. *Colloids Surf., B* **2018**, *171*, 150−158.
(43) Li, Z.; Fan, J.; Tong, C.; Zhou, H.; Wang, W.; Li, B.; Liu, B.; Wang, W. A Smart Drug-Delivery Nanosystem Based on Carboxylated Graphene Quantum Dots for Tumor-Targeted Chemotherapy. *Nanomedicine* **2019**, *14* (15), 2011−2025.
(44) Mohammadian, M.; Kouchakzadeh, H.; Rahmandoust, M.; Mohammadian, T. Targeted Albumin Nanoparticles for the Enhancement of Gemcitabine Toxicity on Cancerous Cells. *J. Drug Delivery Sci. Technol.* **2020**, *56*, No. 101503.
(45) Yang, Z.; Zhang, N.; Ma, T.; Liu, L.; Zhao, L.; Xie, H. Engineered Bovine Serum Albumin-Based Nanoparticles with PH-Sensitivity for Doxorubicin Delivery and Controlled Release. *Drug Delivery* **2020**, *27* (1), 1156−1164.
(46) Gharbavi, M.; Johari, B.; Eslami, S. S.; Mousazadeh, N.; Sharafi, A. Cholesterol-Conjugated Bovine Serum Albumin Nanoparticles as a Tamoxifen Tumor-Targeted Delivery System. *Cell Biol. Int.* **2020**, *44* (12), 2485−2498.

https://doi.org/10.1021/acsomega.3c09608
ACS Omega 2025, 10, 102−113

(47) Azizi, S.; Nosrati, H.; Danafar, H. Simple Surface Functionalization of Magnetic Nanoparticles with Methotrexate-Conjugated Bovine Serum Albumin as a Biocompatible Drug Delivery Vehicle. *Appl. Organomet. Chem.* **2020**, *34* (4), 1−9.
(48) Karaagac, O.; Kockar, H. A Simple Way to Obtain High Saturation Magnetization for Superparamagnetic Iron Oxide Nanoparticles Synthesized in Air Atmosphere: Optimization by Experimental Design. *J. Magn. Magn. Mater.* **2016**, *409*, 116−123.
(49) Yeniyurt, Y.; Kilic, S.; Güner-Yılmaz, O. Z.; Bozoglu, S.; Meran, M.; Baysak, E.; Kurkcuoglu, O.; Hizal, G.; Karatepe, N.; Batirel, S.; Güner, F. S.Fmoc-PEG Coated Single-Wall Carbon Nanotube Carriers by Non-Covalent Functionalization: An Experimental and Molecular Dynamics Study. *Front. Bioeng. Biotechnol.***2021**, *9* (May). .
(50) Datsyuk, V.; Kalyva, M.; Papagelis, K.; Parthenios, J.; Tasis, D.; Siokou, A.; Kallitsis, I.; Galiotis, C. Chemical Oxidation of Multiwalled Carbon Nanotubes. *Carbon N. Y.* **2008**, *46* (6), 833−840.
(51) Wu, H.; Shi, H.; Wang, Y.; Jia, X.; Tang, C.; Zhang, J.; Yang, S. Hyaluronic Acid Conjugated Graphene Oxide for Targeted Drug Delivery. *Carbon N. Y.* **2014**, *69*, 379−389.
(52) Ma, N.; Liu, J.; He, W.; Li, Z.; Luan, Y.; Song, Y.; Garg, S. Folic Acid-Grafted Bovine Serum Albumin Decorated Graphene Oxide: An Efficient Drug Carrier for Targeted Cancer Therapy. *J. Colloid Interface Sci.* **2017**, *490*, 598−607.
(53) Sadegh, H.; Shahryari-ghoshekandi, R.; Kazemi, M. Study in Synthesis and Characterization of Carbon Nanotubes Decorated by Magnetic Iron Oxide Nanoparticles. *Int. Nano Lett.* **2014**, *4* (4), 129−135.
(54) Unsoy, G.; Yalcin, S.; Khodadust, R.; Gunduz, G.; Gunduz, U.Synthesis Optimization and Characterization of Chitosancoated Iron Oxide Nanoparticles Produced for Biomedical Applications. *J. Nanoparticle Res.***2012**, *14* (11). .
(55) Wang, X.; Zhao, Z.; Qu, J.; Wang, Z.; Qiu, J. Fabrication and Characterization of Magnetic Fe_3O_4-CNT Composites. *J. Phys. Chem. Solids* **2010**, *71* (4), 673−676.
(56) Gupta, V. K.; Agarwal, S.; Saleh, T. A. Chromium Removal by Combining the Magnetic Properties of Iron Oxide with Adsorption Properties of Carbon Nanotubes. *Water Res.* **2011**, *45* (6), 2207−2212.
(57) Fan, X. J.; Li, X. Preparation and Magnetic Properties of Multiwalled Carbon Nanotubes Decorated by Fe_3O_4 Nanoparticles. *Xinxing Tan Cailiao/New Carbon Mater.* **2012**, *27* (2), 111−116.
(58) Yao, Y.; Miao, S.; Liu, S.; Ma, L. P.; Sun, H.; Wang, S. Synthesis, Characterization, and Adsorption Properties of Magnetic Fe_3O_4@ graphene Nanocomposite. *Chem. Eng. J.* **2012**, *184*, 326−332.
(59) Tsai, P.-A.; Kuo, H.-Y.; Chiu, W.-M.; Wu, J.-H. Purification and Functionalization of Single-Walled Carbon Nanotubes through Different Treatment Procedures. *J. Nanomater.* **2013**, *2013*, No. 937697.
(60) Domagała, K.; Borlaf, M.; Traber, J.; Kata, D.; Graule, T. Purification and Functionalisation of Multi-Walled Carbon Nanotubes. *Mater. Lett.* **2019**, *253*, 272−275.
(61) Yang, Z. F.; Li, L. Y.; Hsieh, C.Te; Juang, R. S. Co-Precipitation of Magnetic Fe3O4 Nanoparticles onto Carbon Nanotubes for Removal of Copper Ions from Aqueous Solution. *J. Taiwan Inst. Chem. Eng.* **2018**, *82*, 56−63.
(62) Liu, Y.; Guo, L.; Huang, H.; Dou, J.; Huang, Q.; Gan, D.; Chen, J.; Li, Y.; Zhang, X.; Wei, Y. Facile Preparation of Magnetic Composites Based on Carbon Nanotubes: Utilization for Removal of Environmental Pollutants. *J. Colloid Interface Sci.* **2019**, *545*, 8−15.
(63) Lu, Y. J.; Wei, K. C.; Ma, C. C. M.; Yang, S. Y.; Chen, J. P. Dual Targeted Delivery of Doxorubicin to Cancer Cells Using Folate-Conjugated Magnetic Multi-Walled Carbon Nanotubes. *Colloids Surfaces B Biointerfaces* **2012**, *89* (1), 1−9.
(64) Keleştemur, S.; Altunbek, M.; Culha, M. Influence of EDC/NHS Coupling Chemistry on Stability and Cytotoxicity of ZnO Nanoparticles Modified with Proteins. *Appl. Surf. Sci.* **2017**, *403*, 455−463.
(65) Patel, V.; Shah, J.; Gupta, A. K. Design and In-Silico Study of Bioimaging Fluorescence Graphene Quantum Dot-Bovine Serum Albumin Complex Synthesized by Diimide-Activated Amidation. *Comput. Biol. Chem.* **2021**, *93* (May), No. 107543.
(66) Castillo, J. J.; Rindzevicius, T.; Novoa, L. V.; Svendsen, W. E.; Rozlosnik, N.; Boisen, A.; Escobar, P.; Martínez, F.; Castillo-León, J. Non-Covalent Conjugates of Single-Walled Carbon Nanotubes and Folic Acid for Interaction with Cells over-Expressing Folate Receptors. *J. Mater. Chem. B* **2013**, *1* (10), 1475−1481.
(67) Jombert, A. S.; Bayazit, M. K.; Coleman, K. S.; Zeze, D. A. Platinum(II)-Coordinated Pyridine-Functionalized Single-Wall Carbon Nanotubes and Electron Transport in Their Films. *ChemNanoMat* **2015**, *1* (5), 353−358.
(68) Pourjavadi, A.; Kohestanian, M.; Streb, C. PH and Thermal Dual-Responsive Poly(NIPAM-Co-GMA)-Coated Magnetic Nanoparticles via Surface-Initiated RAFT Polymerization for Controlled Drug Delivery. *Mater. Sci. Eng., C* **2020**, *108*, No. 110418.
(69) Chen, H.; Yang, W.; Chen, H.; Liu, L.; Gao, F.; Yang, X.; Jiang, Q.; Zhang, Q.; Wang, Y. Surface Modification of Mitoxantrone-Loaded PLGA Nanospheres with Chitosan. *Colloids Surfaces B Biointerfaces* **2009**, *73* (2), 212−218.
(70) Fan, Y.; Su, F.; Li, K.; Ke, C.; Yan, Y. Carbon Nanotube Filled with Magnetic Iron Oxide and Modified with Polyamidoamine Dendrimers for Immobilizing Lipase toward Application in Biodiesel Production. *Sci. Rep.* **2017**, *7*, 1−13.
(71) Zhang, Q.; Zhu, M.; Zhang, Q.; Li, Y.; Wang, H. The Formation of Magnetite Nanoparticles on the Sidewalls of Multi-Walled Carbon Nanotubes. *Compos. Sci. Technol.* **2009**, *69* (5), 633−638.
(72) Andrade del Olmo, J.; Alonso, J. M.; Sáez-Martínez, V.; Benito-Cid, S.; Moreno-Benítez, I.; Bengoa-Larrauri, M.; Pérez-González, R.; Vilas-Vilela, J. L.; Pérez-Alvarez, L.Self-Healing, Antibacterial and Anti-Inflammatory Chitosan-PEG Hydrogels for Ulcerated Skin Wound Healing and Drug Delivery. *Biomater. Adv.***2022**, *139* (March). 212992.
(73) Anirudhan, T. S.; Christa, J.; Binusreejayan. PH and Magnetic Field Sensitive Folic Acid Conjugated Protein−Polyelectrolyte Complex for the Controlled and Targeted Delivery of 5-Fluorouracil. *J. Ind. Eng. Chem.* **2018**, *57*, 199−207.
(74) Dramou, P.; Fizir, M.; Taleb, A.; Itatahine, A.; Dahiru, N. S.; Mehdi, Y. A.; Wei, L.; Zhang, J.; He, H. Folic Acid-Conjugated Chitosan Oligosaccharide-Magnetic Halloysite Nanotubes as a Delivery System for Camptothecin. *Carbohydr. Polym.* **2018**, *197*, 117−127.

https://doi.org/10.1021/acsomega.3c09608
ACS Omega 2025, 10, 102−113